Ultrasound in Med. & Biol., Vol. 34, No. 12, pp. 2009–2018, 2008

0301-5629/08/$–see front matter

ELSEVIER

doi:10.1016/j.ultrasmedbio.2008.05.003

● *Original Contribution*

EXAMINATION OF INERTIAL CAVITATION OF OPTISON IN PRODUCING SONOPORATION OF CHINESE HAMSTER OVARY CELLS

MONICA M. FORBES,* RYAN L. STEINBERG* and WILLIAM D. O'BRIEN, JR.*†
*Department of Bioengineering; and †Department of Electrical and Computer Engineering, University of Illinois at Urbana-Champaign, Urbana, IL, USA

(*Received* 17 *October* 2007; *revised* 13 *May* 2008; *in final form* 14 *May* 2008)

Abstract—The objective of this project was to elucidate the relationship between ultrasound contrast agents (UCAs) and sonoporation. Sonoporation is an ultrasound-induced, transient cell membrane permeability change that allows for the uptake of normally impermeable macromolecules. Specifically, this study will determine the role that inertial cavitation plays in eliciting sonoporation. The inertial cavitation thresholds of the UCA, Optison, are compared directly with the results of sonoporation to determine the involvement of inertial cavitation in sonoporation. Chinese hamster ovary (CHO) cells were exposed as a monolayer in a solution of Optison, 500,000 Da fluorescein isothiocyanate-dextran (FITC-dextran), and phosphate-buffered saline (PBS) to 30 s of pulsed ultrasound at 3.15-MHz center frequency, 5-cycle pulse duration and 10-Hz pulse repetition frequency. The peak rarefactional pressure (P_r) was varied over a range from 120 kPa–3.5 MPa, and five independent replicates were performed at each pressure. As the P_r was increased, from 120 kPa–3.5 MPa, the fraction of sonoporated cells among the total viable population increased from 0.63–10.21%, with the maximum occurring at 2.4 MPa. The inertial cavitation threshold for Optison at these exposure conditions has previously been shown to be in the range 0.77–0.83 MPa, at which sonoporation activity was found to be 50% of its maximum level. Furthermore, significant sonoporation activity was observed at pressure levels below the threshold for inertial cavitation of Optison. Above 2.4 MPa, a significant drop in sonoporation activity occurred, corresponding to pressures where >95% of the Optison was collapsing. These results demonstrate that sonoporation is not directly a result of inertial cavitation of the UCA, rather that the effect is related to linear and/or nonlinear oscillation of the UCA occurring at pressure levels below the inertial cavitation threshold. (E-mail: mforbes@uiuc.edu) **© 2008 World Federation for Ultrasound in Medicine & Biology.**

Key Words: **Chinese hamster ovary cells, Sonoporation, Ultrasound contrast agent, Inertial cavitation, Thresholds.**

INTRODUCTION

A significant problem in cancer therapy is the compromised quality of life experienced by the patient because of the side effects of the therapeutic compounds. Delivery of molecular medicine to solid tumors is often inefficient and, as a result, the patient's healthy cells and tissues are subject to the toxic effects of the drugs. Thus, it is important to develop approaches that deliver drugs only to the appropriate cells within the patient in a specific, efficient and safe manner. One such method, termed *sonoporation*, involves the use of ultrasound (US) to enhance cell permeabilization. With this method, it is possible, using US and contrast microbubbles, to noninvasively deliver therapeutic compounds into specific target cells.

Sonoporation alters the permeability of cell membranes in a transient fashion (McNeil 1989), leaving the compounds trapped inside the cell once US exposure is complete. Small compounds (Brayman et al. 1999; Guzman et al. 2001; Keyhani et al. 2001), macromolecules (Bao et al. 1997; Greenleaf et al. 1998; Guzman et al. 2002; Miller et al. 1999; Wyber et al. 1997) and other therapeutic compounds (Harrison et al. 1996; Keyhani et al. 2001; van Wamel et al. 2004; Wu et al. 2006) have successfully been delivered into cells using US. Ultrasound can also deliver protein (Mukherjee et al. 2000; Weimann and Wu 2002) and DNA (Amabile et al. 2001; Lawrie et al. 2000; Miller et al. 2003; Miller and Song 2003) into tissues. Low- and high-frequency US treat-

This work was supported in part by an Illinois Distinguished Fellowship for predoctoral students, by NIH grant F31EB06634 and by NIH grant R37EB02641. Cell culture facilities were provided by the Imaging Technology Group of the Beckman Institute for Advanced Science and Technology at the University of Illinois at Urbana–Champaign.

Address correspondence to: Monica M. Forbes, Beckman Institute, 405 N. Mathews, Urbana, IL 61801. E-mail: mforbes@uiuc.edu

ment of cells in the presence of plasmid DNA has been shown to cause mammalian cell transfection *in vitro* (Bao et al. 1997; Frenkel et al. 2002; Kim et al. 1996; Tata et al. 1997) and *in vivo* (Endoh et al. 2002; Miller et al. 1999, 2003; Taniyama et al. 2002). Thus, sonoporation has great possibilities in both targeted gene and drug delivery.

Little is known about the mechanism of sonoporation, both physically and biologically. Tachibana et al. (1999) and Meheir-Humbert et al. (2005) have shown that large pores form in a cell membrane after US exposure. Schlicher et al. (2006) provided evidence that these membrane disruptions are similar to those formed by other physical stresses and are resealed by an active process of vesicle fusion with the cell membrane. Cellular and molecular damage to human red blood cells occurs as a result of US exposure (Kawai and Iino 2003), although the role this damage plays in pore formation is unknown. It has been shown that the enhanced membrane permeability in sonoporation is transient (Bao et al. 1997; Brayman et al. 1999; McNeil 1989; Taniyama et al. 2002) and the recovery rate does not vary significantly with US parameters or the maximum amplitude of the transmembrane current (Deng et al. 2004). In addition, hyperpolarization of the cell membrane occurs in the presence of US and ultrasound contrast agent (UCA), most likely because of the activation of channels sensitive to mechanical stresses and nonspecific ion channels (Tran et al. 2007). However, this hyperpolarization does not explain the presence of the pores in the membrane.

The presence of a UCA is necessary to induce a significant sonoporation event (Bao et al. 1997; Greenleaf et al. 1998; Kim et al. 1996). This UCA requirement has led to the identification of inertial cavitation (IC), which is the rapid collapse of a bubble, as the probable sonoporation mechanism, theorized by several studies (Bao et al. 1997; Greenleaf et al. 1998; Hwang et al. 2005; Koch et al. 2000; Lai et al. 2006). However, the data provided in the literature are only circumstantial, not direct evidence that collapse cavitation is the sonoporation mechanism. UCAs have a complex dynamic behavior in an ultrasonic field. The major behaviors are linear oscillation, nonlinear oscillation and IC. Determining whether oscillation or IC of UCAs is involved in producing sonoporation is essential for determining the physical phenomenon responsible for this biological effect (Fig. 1).

Most UCAs are gas-filled, encapsulated microbubbles designed to increase acoustic reflectivity. As acoustic waves are incident on the UCA, it grows and shrinks because of the time-varying pressure of the wave. The behavior of the UCA is dependent on US frequency (Ammi et al. 2006b; Chen et al. 2003; Chomas et al. 2001; Giesecke and Hynynen 2003) and peak rarefactional pressure. At low-level acoustic pressure amplitudes, linear oscillation of the UCA occurs. These oscillations lead to local steady flows that are termed microstreaming. When the UCA is close to a cell, this microstreaming can lead to shearing motions on the cell membrane. Theoretical and experimental studies have shown that microstreaming near a cell boundary can adversely affect a cell membrane. The critical stress (in terms of viscous stress) for hemolysis is well defined (Rooney 1970; Williams et al. 1970). In addition, microstreaming from a vibrating Mason horn demonstrated a threshold for enhanced membrane permeability (12 ± 4 Pa at 21.4 kHz) (Wu et al. 2002). Also, under single-bubble controlled conditions (10 kPa at 180 kHz), Marmottant and Hilgerfeldt (2003) demonstrated experimentally that linear microbubble oscillations were sufficient to rupture lipid membranes because of large-velocity gradients. Thus, microstreaming as a result of linear oscillation of UCAs could play a role in sonoporation.

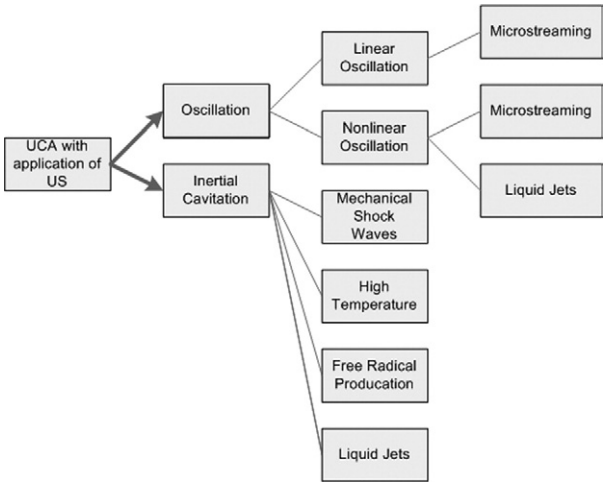

Fig. 1. The numerous UCA responses to US and the possible bioeffects of each response, thus emphasizing the critical junction of IC *vs.* oscillation in determining the mechanism for sonoporation.

At higher pressure amplitudes, UCAs exhibit nonlinear oscillation. During these conditions, the UCA expands slowly during rarefaction and is followed by a rapid contraction, but not collapse, during compression. Nonlinear oscillation produces microstreaming, as well as the potential for liquid jets (also known as *microjetting*). Liquid jets are formed as a result of the asymmetric behavior of the UCA in the presence of a pressure gradient near a surface, such as a cell. These jets can then impinge on the cell membrane at high speeds. Liquid jets provide increased transport of heat and gas by streaming and have the capacity to puncture the cell membrane, producing openings that could allow for the transport of extracellular material into the cell (Prentice et al. 2005).

But, the formation of jets is a bit chaotic (Prosperetti 1997).

As the pressure amplitude is increased further, the maximum-to-initial diameter ratio reaches 2, a common criterion for UCA collapse (Church 2005; Flynn 1975; Flynn and Church 1988). This collapse is termed IC because the UCA motion is dominated by the inertia of the liquid. For a shelled UCA, this violent collapse causes the shell to fragment, releasing the encapsulated gas and possibly generating daughter/free bubbles that can also oscillate. The violent collapse of the bubble during IC produces many mechanical effects and chemical agents that could cause bioeffects. Some of the consequences of collapse are mechanical shock waves, a bubble temperature that may reach thousands of degrees Kelvin (4,300 to 5,000°K) (Didenko et al. 1999; Suslick 2001), microjetting and free radical production (FRP). FRP is caused by the dissociation of water vapor during contraction of the UCA and can mediate chemical changes. However, it has been shown that FRP is not required for transfection (Lawrie et al. 2003).

Sonoporation is a promising drug delivery and gene therapy technique, limited chiefly by a lack of understanding regarding the biophysical mechanism that causes the cell membrane permeability change. The objective of this project was to elucidate the relationship between UCAs and sonoporation, specifically determining the role IC plays in sonoporation.

MATERIALS AND METHODS

Cell culture

Chinese hamster ovary (CHO) cells (American Type Culture Collection [ATCC], Manassas, VA, USA) were cultured in F-12K medium (ATCC) with 10% v/v fetal bovine serum (ATCC), 1% penicillin/streptomycin (Sigma-Aldrich, St. Louis, MO, USA) and 0.1% Fungizone (Invitrogen, Carlsbad, CA, USA). Nonhuman cells purchased from ATCC, cultured and used with no animal involvement do not need IACUC approval. The cells were propagated as a monolayer in 75 cm^3 tissue culture flasks at 37°C and a humidified atmosphere of 5% CO_2. All work, except the US exposure, was performed in a biological safety cabinet.

Contrast agent

Optison (Amersham Health Inc., Princeton, NJ, USA) contains perfluoropropane and is stabilized by a human serum albumin shell, with a mean diameter between 2 and 4.5 μm. The concentration of Optison is 5 to 8×10^8 mL^{-1} gas bodies.

Ultrasound exposure vessels and cell preparation

The sample vessel was a 96-well cell culture microplate (BD Falcon, San Jose, CA, USA) constructed from medical-grade polystyrene. Each well is flat bottomed, holds 0.37 mL and has a diameter of 6.4 mm, 4.25 times the −6 dB focal beamwidth of the 3.15-MHz transducer. The open face of the microplate was covered by plastic cling wrap, forming a barrier between the external water bath and internal cell solution, as well as an acoustic window for the US to pass unperturbed into the well.

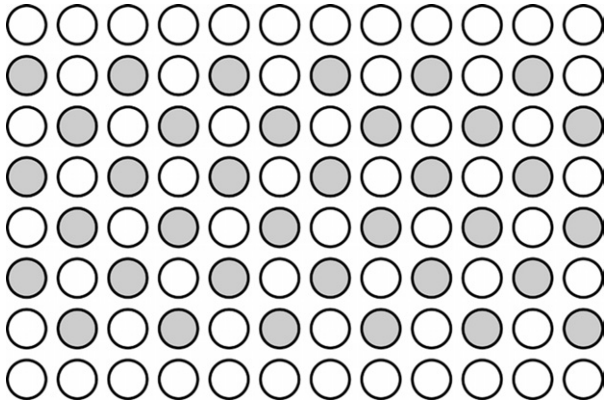

Fig. 2. The loading pattern of the 96-well microwell plate. Note that the top and bottom rows are left empty and every other well is loaded.

For preparation of an experiment, CHO cells were harvested with 2-mL trypsin-EDTA (Sigma-Aldrich), and 0.3×10^6 cells/mL in 0.37 mL of growth medium were added to each well of one clean, sterilized exposure vessel. Thirty-six wells were loaded with cells and the loading configuration is schematically displayed in Fig. 2. Cells were loaded in every other well to prevent interaction between adjacent wells (*e.g.*, leaking of medium from one well to the next and possible mechanical interactions). The top and bottom rows of the plate were left empty to provide a location for clamping the plate into the holder in the degassed water tank. The vessel was incubated overnight to allow the seeded cells to settle to the bottom of each well, thus forming the monolayer of >90% confluence. On the day of the experiment, the growth medium was removed and the monolayer rinsed twice with phosphate-buffered saline (PBS) to remove any dead cells and debris.

The exposure medium added to each well contained fluorescein isothiocyanate-dextran (FITC-dextran) (FD500S, Sigma-Aldrich), with an average molecular weight (MW) of 500,000 Da. The FITC-dextran is normally unable to cross the cell membrane, and thus used as the marker for change in cell membrane permeability. A volume of 0.05 mL FITC-dextran solution (25 mg/mL in PBS), 8.80 μL Optison and 0.312 mL PBS were added to each well. The plate was then sealed with plastic cling wrap. Any wells con-

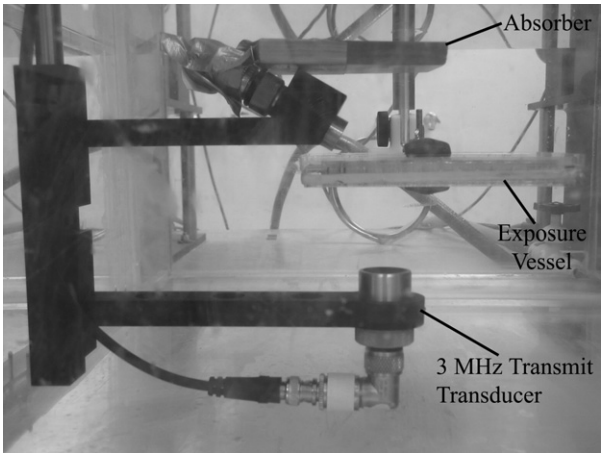

Fig. 3. The experimental setup.

taining air bubbles were excluded from the experiment.

The vessel was placed in a room temperature, degassed water bath, with the plastic cling wrap located near the transducer (Fig. 3). Thus, the monolayer was on the back window of the chamber, allowing the UCAs to rise to the monolayer because of buoyancy and be pushed toward the monolayer by the radiation force. The vessel was located so the focus of the transducer was positioned at the bottom of the well, where the cells were located. Also, a water level was used to align the vessel with the horizontal plane. Before each exposure, the vessel was centered with respect to the US beam, so exposure occurred at the center of the exposed well; this centering process took approximately 5 min. The first well was exposed approximately 30 s after completion of alignment. Each well was independently exposed or sham exposed (US turned off) at the predetermined conditions. The order of well exposure was varied to avoid any influences regarding the order of exposure.

Ultrasound exposure

US was produced by a 3.15-MHz f/3 19 mm–diameter single-element focused transducer (Valpey Fisher, Hopkinton, MA, USA). The −6 dB beamwidth at the focus was 1.5 mm, and the depth of focus was 29 mm, both measured quantities (Raum and O'Brien 1997). For exposure, the transducer was mounted in a degassed water bath and aimed upward at the exposure chamber located at the focus. Sinusoidal tone bursts were generated by a pulser–receiver (Ritec RAM5000, Warwick, RI, USA) for a pulse duration (PD) of 5 cycles, pulse repetition frequency (PRF) of 10 Hz and exposure duration of 30 s. The peak rarefactional pressure (P_r) was varied over a range from 0.12–3.5 MPa, and five independent replicates were performed at each P_r value (0, 0.122, 0.204, 0.436, 0.908, 1.31, 1.74, 2.40, 2.69 and 3.50 MPa). This P_r range encompassed the threshold range for Optison collapse, 0.77–0.83 MPa (Ammi 2006; Ammi et al. 2006b).

The calibrated pressure amplitude at the focus was varied using the pulser–receiver's output control settings. To obtain smaller changes in the pressure amplitude, a step-variable attenuation was used. The pressure waveforms were calibrated at the field's focus for each exposure condition. Calibrations were routinely performed according to well-established calibration techniques (Preston et al. 1983; Zachary et al. 2001) using an NPL-calibrated polyvinylidene difluoride bilaminar shielded membrane hydrophone (diameter of the active element: 0.5 mm, Marconi 699/1/00001/100; GEC Marconi Ltd., Great Baddow, UK). The hydrophone was located in the field's focus at the same position that the exposure vessel was located during experiments.

The attenuation of the plastic cling wrap and reflection coefficient of the bottom of the vessel were found by measuring the US amplitude of the polystyrene and/or plastic cling wrap in comparison with a Plexiglas block with known reflection. The attenuation of the plastic cling wrap was negligible and the pressure reflection coefficient of the polystyrene was 0.33. This reflection was taken into account. The peak rarefactional pressure reported here included the measured pressure *via* calibration, without the microwell plate present, plus the pressure of the reflected wave caused by the reflection that occurs from the polystyrene when the microwell is present. In addition, an absorber was placed above the microplate to prevent reflection from the water–air interface at the top of the tank from interfering with the exposure conditions (Fig. 3).

Postexposure analysis

After exposure, the vessel was removed from the water bath. The exposure medium in each of the wells was transferred to correspondingly labeled microcentrifuge tubes and placed on ice. Trypsin-EDTA (0.1 mL) was added to the monolayer in each well, and after 5 min the trypsinized cells were added to the same microcentrifuge tube as the exposure medium. Thus, the microcentrifuge tube contains all the cells in the monolayer and any cells that may have been dislodged from the monolayer during the procedure for a single well of the microwell plate. Each cell suspension was immediately washed twice with 1 mL cold PBS to avoid pinocytosis. Viewing of the cells with fluorescence microscopy verified that the FITC-dextran was distributed uniformly throughout the cytoplasm and not confined to small intracellular vacuoles, as would be expected for pinocytosis or phagocytosis (results not shown). To assess cell viability, 1 μL propidium iodide (PI) (Sigma-Aldrich) was added to each sample. Samples were analyzed

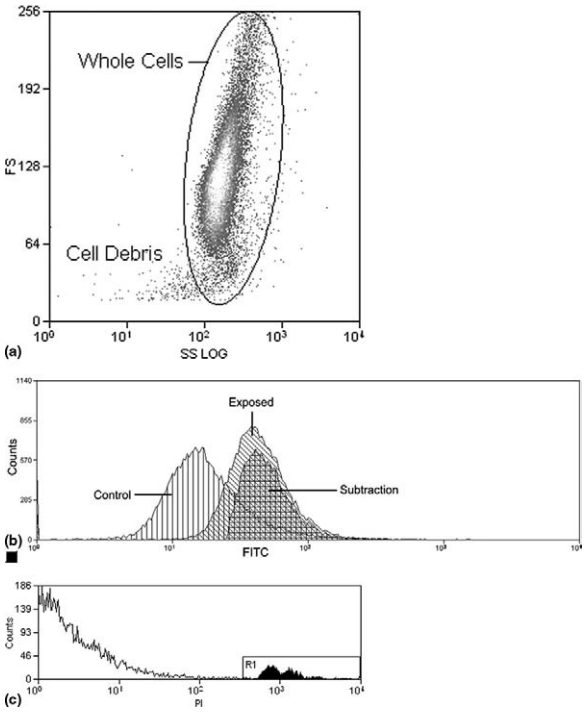

Fig. 4. (A) Example of the side-scatter (SS) *vs.* forward scatter (FS) histogram obtained by the flow cytometer. The cells within the ellipsoid region are the whole cells, viable and nonviable, that are used in the sonoporation analysis. All points not located within the ellipse are designated as cell debris. (B) Example of the FITC histogram obtained by the flow cytometer. The control histogram is from the sham-exposed sample (US turned off) and the exposed histogram is from the sample exposed to US. The subtraction histogram is the result when subtracting the control histogram from the exposed histogram. The number of cells in the subtraction histogram divided by the number of cells in the exposed histogram is the percentage of sonoporated cells. (C) Example of the PI histogram. The region R1 represents the cells stained with PI and designated as nonviable.

using flow cytometry (Beckman Coulter, Inc. Epics XL-MCL, Fullerton, CA, USA).

Fluorescent probes were excited at 488 nm by an argon laser and the emitted light was detected at 520 nm for FITC and 608 nm for PI. A minimum of 18,000 cells were examined in each sample. Figure 4a shows an example of the side-scatter *vs.* forward-scatter histogram obtained by the flow cytometer, with the whole cell and cell debris populations labeled. Results from flow cytometry are expressed in percentages of positively labeled cells, using the software program Summit v3.1 For MoFlo® Acquisition and Sort Control (Cytomation Inc., Fort Collins, CO, USA). The percent of positive cells is relative to whole cells only, as debris from cells was ignored. Cell debris consists of parts of cell membrane, mitochondria, other organelles, dust particles, *etc.* The number of cells contributing to this debris is not known, thus for this discussion of sonoporation, the debris does not provide any additional information. The data obtained provided the percent of fluorescent cells and dead cells in the entire population. Figure 4b shows an example of the FITC histogram. The control histogram is from the sham-exposed sample (US turned off), and the exposed histogram is from the sample exposed to US. To determine the sonoporated cells, the control histogram is subtracted from the exposed histogram. Both the control histogram and the exposed histogram are normalized to 18,000 counts. The number of cells in the subtraction histogram is divided by the number of cells in the exposed histogram to obtain the percentage of sonoporated cells. FITC-dextran does not bind to the cell membrane (McNeil 1989), so fluorescence of a cell indicates internalized material (*i.e.*, sonoporation). Figure 4c shows an example of the PI histogram. The cells in region R1 are those that had PI uptake and were designated as nonviable.

Acoustic pressure thresholds for collapse of Optison microbubbles

A passive cavitation detector (PCD) (Madanshetty et al. 1991) was used to determine collapse thresholds of Optison in degassed water (Ammi 2006; Ammi et al. 2006b). A 13-MHz measured center-frequency focused transducer (12.7-mm diameter and 15.4-mm focal length), mounted confocal and at a 115° angle to the transmit beam axis, was used to passively collect emissions from the bubbles injected into degassed water. The −6 dB field limits were determined for each transducer by measurement (Raum and O'Brien 1997). The approximate confocal volume was 0.12 mm^3. The outputs from both transducers were amplified (44 dB), digitized (12-bit, 200 MHz, Strategic Test digitizing board UF 3025, Cambridge, MA, USA) and saved to a computer. The data were processed off-line using MATLAB (The MathWorks, Natick, MA, USA) .

The signals detected from the PCD revealed post-excitation acoustic emissions with broadband spectral content. The observed acoustic emissions were consistent with the acoustic signature that would be anticipated from inertial collapse followed by "rebounds," when a microbubble ruptures and thus generates daughter/free bubbles that grow and collapse. Logistic regression analysis (Agresti 1996) was used to analyze the dependence of ruptured microbubble occurrence rates on P_r, and both the first IC event and the 5% occurrence rate were used to quantify the shell rupture (IC) thresholds; an automated algorithm applied to the PCD signals detected the number of IC events out of 128 data realizations at each acoustic pressure level.

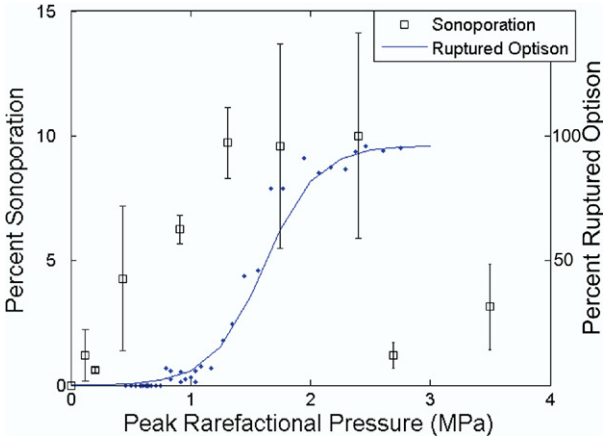

Fig. 5. Sonoporation of CHO cells exposed at 3.15 MHz, 5 cycles, 10 Hz and for 30 s compared with the occurrence of ruptured Optison. The collapse threshold for Optison occurs at 0.83 MPa.

RESULTS

CHO cells exposed to US in the presence of the UCA Optison were observed, by means of FITC-dextran internalization, to have undergone sonoporation. A threshold-type study examining sonoporation activity as a function of P_r was performed. Over the P_r range, 120 kPa–3.5 MPa, the fraction of sonoporated cells among the total viable population varied from 0.63–10.2%, with the sonoporation activity increasing as P_r increased, up to a maximum occurring at 2.4 MPa (Fig. 5). The error was calculated using standard error of measurement for the five independent replicate samples at each P_r. It is important to note that only 5.5% of the cells in each well were exposed within the −6 dB beamwidth at the 3.15-MHz transducer focus (1.5 mm); however the entire well was sampled for sonoporation.

The 2.8-MHz 5-cycle collapse data of Optison are also plotted on Fig. 5 (data obtained from Fig V.6 in Ammi [2006]; see also Ammi et al. [2006a] to show the relationship between sonoporation and IC). The percentage of observed bubbles that underwent collapse at each P_r is displayed. Two 2.8-MHz 5-cycle thresholds were determined for Optison: first IC event and 5% occurrence rate using logistic regression analysis. The first IC event was at 0.77 MPa and the 5% occurrence rate was at 0.83 MPa (Ammi 2006). First IC event thresholds at 0.9, 2.8 and 4.6 MHz for 3, 5 and 7 cycles are graphically represented in Ammi et al. (2006) and show that the first IC event thresholds increase as frequency increases; this frequency trend suggests that at 3.15 MHz, the collapse thresholds would be slightly greater than those at 2.8 MHz. Around this threshold pressure (0.77 to 0.83 MPa), sonoporation had already reached >50% relative to the maximum sonoporation activity, indicating that significant sonoporation is taking place at P_r levels where IC of Optison was not occurring.

At P_r >2.4 MPa, a significant drop in sonoporation activity was observed. This decrease corresponds to the pressure where >95% of the Optison was collapsing (Fig. 5). The percentage of nonviable cells at each P_r is plotted in Fig. 6. For the range of P_r examined, 120 kPa–3.5 MPa, the nonviable cells varied between 0.74% and 3.9%, with no distinct pattern emerging with respect to P_r. This emphasizes that sonoporation is not immediately lethal to the cells and that cell death is not related to the activity of the UCA, nor is cell death a contributor for the drop in sonoporation seen above 2.4 MPa. In addition, the percentage of total items counted by the flow cytometer that were classified as cell debris is presented in Fig. 7. At the higher pressure settings, where a drop in sonoporation activity occurred, there is no increased percentage of cell debris. Thus, the drop in sonoporation at these higher pressures is also not because of increased destruction of cells resulting in increased cell debris.

The CHO cells were exposed to US without Optison added to the solution. Figure 8 presents the percentage of sonoporated cells without Optison compared with the percentage of sonoporated cells with Optison for 3 P_r levels (0.204, 1.74 and 2.69 MPa). The percentage of sonoporated cells without Optison is not significantly different from the control sample (US off). However, the percentage of sonoporated cells with Optison differs from the samples without Optison and the control samples for a P_r of 1.74 MPa.

DISCUSSION

The role of IC as the sonoporation mechanism has previously not been elucidated with direct evidence. Hal-

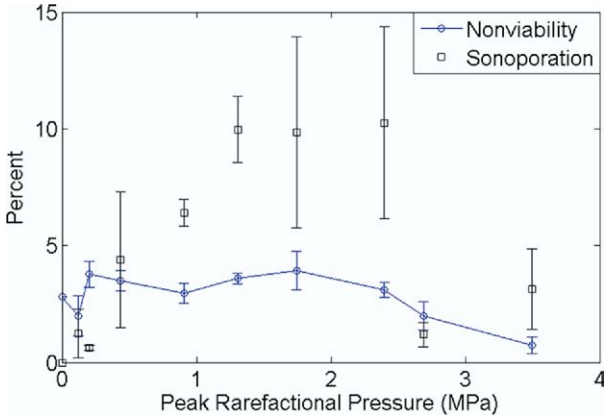

Fig. 6. Percentage of nonviable cells exposed at 3.15 MHz, 5 cycles, 10 Hz and for 30 s in the presence of Optison compared with the sonoporation activity for the same exposure conditions.

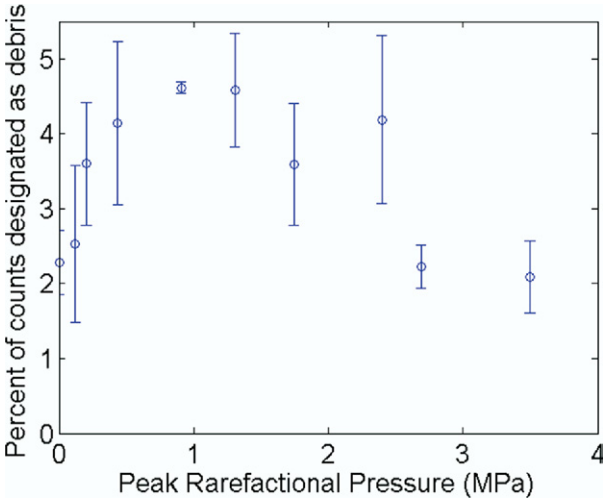

Fig. 7. Percentage of items counted by flow cytometer that were designated as cell debris from samples exposed at 3.15 MHz, 5 cycles, 10 Hz and for 30 s in the presence of Optison.

low et al. (2006) did show that acoustic cavitation correlates well with sonoporation activity through a simultaneous monitoring of inertial cavitation dose and cell exposure. However, an integration of the average broadband noise was used as the inertial cavitation dose. Further, this method is unable to quantify the amount of IC and UCA oscillation. This quantification becomes important when looking at exposure conditions around the threshold for collapse. The experimental observations reported herein provide evidence that sonoporation is not directly caused by IC of UCAs, using characteristic rebounds that occur when a microbubble ruptures as the criteria for the IC event. This is most apparent in comparing the collapse threshold of Optison with the sonoporation response to P_r, as in Fig. 5. The threshold for Optison collapse is around a P_r of 0.77–0.83 MPa, hence below this pressure range, few, if any, microbubbles undergo collapse. However, below this collapse threshold, significant sonoporation is occurring. Furthermore, at the threshold for Optison collapse, sonoporation activity is half of the maximum observed activity. These results demonstrate that sonoporation is occurring while Optison is intact, thus IC is not the mechanism responsible for sonoporation.

To verify that sonoporation was a UCA-mediated event, samples were exposed to US without Optison present. Streaming within the well because of US could potentially impact the cell membrane. In addition, cells that have been dislodged from the bottom of the well from the US could have a membrane permeability change because of this dislodging process (McNeil 1989). If either of these mechanisms were responsible for the uptake of FITC-dextran, then samples exposed to US without UCA would show uptake. However, as seen in Fig. 8, without Optison present, sonoporation activity is not observed. Therefore, the sonoporation observed in these studies was mediated by UCA activity.

The exposure-dependent sonoporation activity between 120 kPa and 2.4 MPa, a P_r range that transitions the UCAs' response from linear to nonlinear to IC, suggests a mechanism that is also exposure dependent throughout this range of rarefactional pressures. It is likely that microstreaming is exposure dependent between 120 kPa and 2.4 MPa, and supported by the observation of Marmottant and Hilgenfeldt (2003). The shear stress caused by microstreaming from microbubble oscillation is

$$S = \frac{2\pi\eta f\varepsilon_o^2}{A\delta} \quad (1)$$

where δ is the boundary layer thickness, A is the initial bubble radius, η is the shear viscosity of the medium, f is the frequency and ε_o is the radial oscillation amplitude (Rooney 1970). The ε_o is dependent on P_r (Emmer et al. 2007; Marmottant et al. 2005), with larger microbubble oscillation amplitudes occurring as P_r is increased. Marmottant et al. (2005) presented experimental results of a 0.8-μm radius BR14 UCA oscillating in a single 5-cycle pulse of 2 MHz US. At P_r = 200 kPa, ε_o was approximately 0.15 μm; at P_r = 250 kPa, ε_o was approximately 0.2 μm; and at P_r = 300 kPa, ε_o was approximately 0.35 μm. Emmer et al. (2007) presented similar results using a 3.5-μs pulse at 1.7 MHz. For BR14 UCA of 3 μm, at P_r = 100 kPa, ε_o was approximately 0.08 μm; at P_r = 200 kPa, ε_o ranged from 0.23–0.6. μm; and at P_r = 250 kPa, ε_o ranged from 0.38–0.78 μm. Hence, as P_r in-

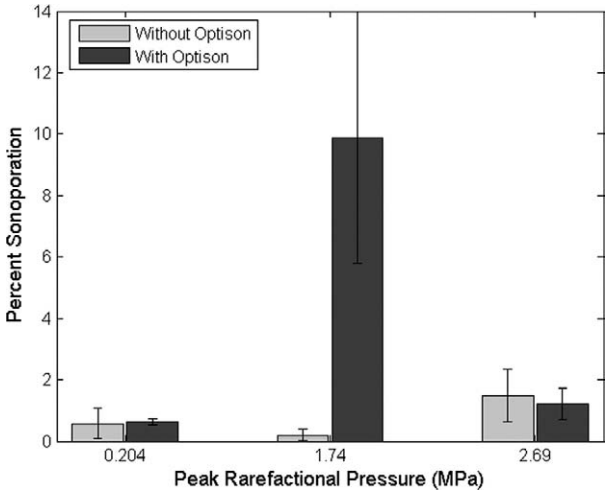

Fig. 8. Percentage of sonoporated cells exposed at 3.15 MHz, 5 cycles, 10 Hz and for 30 s without Optison compared with the percentage of sonoporated cells with Optison for P_r of 0.204, 1.74 and 2.69 MPa.

creases, ε_o increases, resulting in an increased shear stress. Therefore, the shear stress as a result of microstreaming is dependent on the applied P_r, with increased microstreaming occurring with increased P_r.

Using this definition of shear stress it is possible to demonstrate that microstreaming around UCAs has the potential to induce sonoporation. Several studies have presented observations of streamlines that develop around a vibrating bubble (Marmottant and Hilgenfeldt 2003; Rooney 1970). Through visual observation, the smallest streamline traced was approximately one and two times the circumference of the bubble, respectively. Let us assume that one circuit of the streamline is sufficient for a fully developed streaming flow to develop around a bubble that is initially at rest and then excited by US. If we use the more recent value, then the distance the fluid must travel is $2\pi A$. The limiting tangential fluid velocity at the surface of the bubble is given by (Coakley and Nyborg 1978)

$$U_L = \frac{2\pi f \varepsilon_o^2}{A} \tag{2}$$

Thus, the time to complete one circuit of the smallest streamline is

$$\tau = \frac{2\pi A}{U_L} \tag{3}$$

If we assume the radial oscillation amplitude is where the UCA undergoes inertial cavitation (2 times the initial radius), ξ_o is A. Thus, τ becomes

$$\tau = \frac{1}{f}. \tag{4}$$

The frequency used in this study was 3.15 MHz, therefore the time for microstreaming to develop around a bubble is 0.32 μs. The time duration for a single pulse in this study was 1.67 μs, thus microstreaming would develop within a single pulse of US.

The shear stress, S, can be calculated for this study. The boundary layer thickness, δ, is defined as

$$\delta = \left(\frac{\eta}{\rho \pi f}\right)^{\frac{1}{2}} \tag{5}$$

where ρ is the density of the medium (Coakley and Nyborg 1978). The exposure medium used in this study has a concentration of 0.30% dextran with a 500 kDa molecular weight, which results in a shear viscosity around 0.002–0.003 Pa-s (Nyborg 1975). If we assume a shear viscosity of 0.002 Pa-s, δ is 0.45 μm. If the initial radius of the UCA is 2 μm, S is calculated to be 1.76×10^5 dyn-cm^{-2} using eqn (1). Rooney (1972) found that, at the threshold stress for hemoglobin release of red blood cells, the duration of the applied stress was 25 μs. In this study, the time of the applied stress of a single pulse was 1.67 μs; however, as the relaxation time of biological materials is long under these conditions, it can be assumed that successive pulses would have a cumulative effect on streaming. Thus, 15 pulses would be required to achieve a 25-μs applied stress, which is approximately 1.5 s of exposure. The ED for this study was 30 s, so it is reasonable that a biologically active microstreaming flow pattern is developed during the exposure. Ammi et al. (2006b) presented evidence that Optison microbubbles collapse within a single pulse; thus, when a UCA undergoes collapse, there is not sufficient time for microstreaming to impact the cells and, hence, no sonoporation occurs.

At $P_r > 2.4$ MPa, a drop in sonoporation activity occurs. At these P_r values (2.7 and 3.5 MPa), >95% of the bubbles are collapsing quite rapidly. Because of their rapid collapse within a single pulse, the UCAs are not present to oscillate and contribute to microstreaming. Thus, at higher P_r, microstreaming will be minimized. A similar drop in sonoporation activity was seen in Hallow et al. (2006) using 1.7 vol% Optison, 1.1 MHz and 3-s exposure duration. The percentage of viable cells increased as the pressure was increased from 0.5 MPa to 1.7 MPa. From 1.7 MPa to 2.0 MPa, the percentage of sonoporated cells decreased from 20% to around 7%. Furthermore, it has been shown that as the percentage of Optison bubbles destroyed increases, the molecular uptake of macromolecules by cells in suspension was found to decrease (Kamaev et al. 2004).

The drop in sonoporation activity seen in this study does not have a corresponding increase in the percentage of nonviable cells or an increase in lysed cells and debris. The results presented here suggest that increased cell death is not a cause of this decreased sonoporation. However, several studies have shown that at higher acoustic pressures, cell viability does decrease (Bao et al. 1997; Hallow et al. 2006). The major difference between those studies and this one is the configuration of the cells. This study was performed as a monolayer, whereas the cited studies were suspension cells.

Published reports that have rigorously examined the behavior of liquid jets are scarce and none replicate the situation in this study. However, results suggest that liquid jets are a less likely explanation for the sonoporation results presented in this paper. Kodama and Takayama (1998) investigated the interaction of shock waves with bubbles attached to rat livers. They observed that liquid jets as a result of oscillating bubbles are capable of penetrating into rat livers, and the penetration depth of the liquid jet rapidly decreased with decreasing equilibrium radius of the bubble. The smallest bubble examined had a radius of 100 μm, whereas Optison has a mean radius of 2–4.5 μm. In addition, jet formation shows some irregularities near the threshold. Because of this irregularity, we do not anticipate jet formation could be responsible for the trends in sonopora-

tion results observed here. Prentice et al. (2005) provided evidence that microjets from shelled microbubbles can produce pits on the surface of a cell membrane. However, they do not show that macromolecules are able to pass into the cell through those pits. In addition, they concluded that the extent of those microjet-induced pits would suggest that lysis of the cell was inevitable, and the exposed cells in this study do not undergo increased lysis. Literature has shown that microjets do have the potential to contribute to sonoporation, but in this study they are unlikely to be the dominant mechanism.

The evidence provided suggests that the sonoporation effect was caused by linear or nonlinear oscillation of the UCA. These responses occur at lower pressure amplitudes and could thus explain the presence of sonoporation at the lower pressure levels. Therefore, we conclude that IC is not the responsible mechanism for sonoporation, and we hypothesize that microstreaming as a result of microbubble oscillations is principally responsible.

REFERENCES

Agresti A. An Introduction for Categorical Analysis. New York: Wiley, 1996.

Amabile PG, Lewis JM, Lewis TN. High-efficiency endovascular gene delivery via therapeutic ultrasound. J Am Coll Cardiol 2001;37: 1975–1980.

Ammi AY. Detection et caracterisation de la destruction des microbulles de produit de contrast e ultrasonore (Detection and characterization of the destruction of ultrasound contrast agents). Doctoral thesis, University of Paris VI; 2006. (In English).

Ammi AY, Bridal SL, Mamou J, Wang GI, O'Brien WD Jr. Automatic detection of ultrasound contrast microbubble shell rupture. Proc 2006 IEEE Ultrason Symp 2006a:297–300.

Ammi AY, Cleveland RO, Mamou J, Wang GI, Bridal SL, O'Brien WD Jr. Ultrasonic contrast agent shell rupture detected by inertial cavitation and rebound signals. IEEE Trans Ultrason Ferroelectr Freq Control 2006b;53:126–136.

Bao S, Thrall BD, Miller DL. Transfection of a reporter plasmid into cultured cells by sonoporation *in vitro*. Ultrasound Med Biol 1997; 23:953–959.

Brayman AA, Coppage ML, Vaidya S, Miller MW. Transient poration and cell surface receptor removal from human lymphocytes *in vitro* by 1-MHz ultrasound. Ultrasound Med Biol 1999;25:999–1008.

Chen WS, Brayman AA, Matula TJ, Crum LA, Miller MW. The pulse length-dependence of inertial cavitation dose and hemolysis. Ultrasound Med Biol 2003;29:739–748.

Chomas JE, Dayton P, May D, Ferrara K. Threshold of fragmentation for ultrasonic contrast agents. J Biomed Optics 2001;6:141–50.

Church CC. Frequency, pulse length, and the mechanical index. Acoust Res Lett Online 2005;6:162–168.

Coakley WT, Nyborg WL. Cavitation; Dynamics of Gas Bubbles; Applications. In: Ultrasound: Its Applications in Medicine and Biology. Amsterdam, The Netherlands: Elsevier Scientific Publishing Company, 1978:77 –159.

Deng CX, Sieling F, Pan H, Cui J. Ultrasound-induced cell membrane porosity. Ultrasound Med Biol 2004;30:519–526.

Didenko YT, McNamera III WB, Suslick KS. Hot spot conditions during cavitation in water. J Am Chem Soc 1999;24:5817–5818.

Emmer M, van Wamel A, Goertz D, de Jong N. The onset of microbubble vibration. Ultrasound Med Biol 2007;33:941–949.

Endoh M, Koibucki N, Sato M. Fetal gene transfer by intrauterine injection with microbubble-enhanced ultrasound. Mol Ther 2002; 5:501–508.

Flynn HG. Cavitation dynamics. II. Free pulsations and models for cavitation bubbles. J Acoust Soc Am 1975;58:1160–1170.

Flynn HG, Church CC. Transient pulsations of small gas bubble in water. J Acoust Soc Am 1988;84:985–998.

Frenkel PA, Chen S, Thai T, Shohet RV, Grayburn PA. DNA-loaded albumin microbubbles enhance ultrasound-mediated transfection *in vitro*. Ultrasound Med Biol 2002;28:817–822.

Giesecke T, Hynynen K. Ultrasound-mediated cavitation thresholds of liquid perfluorocarbon droplets *in vitro*. Ultrasound Med Biol 2003; 29:1359–1365.

Greenleaf WJ, Bolander ME, Sarkar G, Goldring MB, Greenleaf JF. Artificial cavitation nuclei significantly enhance acoustically induced cell transfection. Ultrasound Med Biol 1998;24:587–595.

Guzman HR, Nguyen DX, McNamera A, Prausnitz MR. Equilibrium loading of cells with macromolecules by ultrasound: Effects of molecular size and acoustic energy. J Pharm Sci 2002;91:1693–1701.

Guzman HR, Nguyen DX, Sohail K, Prausnitz MR. Ultrasound-mediated disruption of cell membranes I. Quantification of molecular uptake and cell viability. J Acoust Soc Am 2001;110:588–596.

Hallow DM, Mahajan AD, McCutchen TE, Prausnitz MR. Measurement and correlation of acoustic cavitation with cellular bioeffects. Ultrasound Med Biol 2006;32:1111–1122.

Harrison GH, Balcer-Kubiczek E, Gutierrez PL. In vitro mechanisms of chemopotentiation by tone-burst ultrasound. Ultrasound Med Biol 1996;22:355–362.

Hwang JH, Brayman AA, Reidy MA, Matula TJ, Kimmey MB, Crum LA. Vascular effects induced by combined 1-MHz ultrasound and microbubble contrast agent treatments *in vivo*. Ultrasound Med Biol 2005;31:553–564.

Kamaev PP, Hutcheson JD, Wilson ML, Prausnitz MR. Quantification of Optison bubble size and lifetime during sonication dominant role of secondary cavitation bubbles causing acoustic bioeffects. J Acoust Soc Am 2004;115:1818–1825.

Kawai N, Iino M. Molecular damage to membrane proteins induced by ultrasound. Ultrasound Med Biol 2003;29:609–614.

Keyhani K, Guzman HR, Parsons A, Lewis TN, Prausnitz MR. Intracellular drug delivery using low-frequency ultrasound: Quantification of molecular uptake and cell viability. Pharm Res 2001;18:1514.

Kim HJ, Greenleaf JF, Kinnick RR, Bronk JT, Bolander ME. Ultrasound-mediated transfection of mammalian cells. Human Gene The 1996;7:1339–1346.

Koch S, Pohl P, Cobet W, Rainov NG. Ultrasound enhancement of liposome-mediated cell transfection is caused by cavitation effects. Ultrasound Med Biol 2000;26:897–903.

Kodoma T, Takayama T. Dynamic behavior of bubbles during extracorporeal shock-wave lithotripsy. Ultrasound Med Biol 1998;24: 723–738.

Lai C, Wu C, Chen C, Li P. Quantitative relations of acoustic inertial cavitation with sonoporation and cell viability. Ultrasound Med Biol 2006;12:1931–1941.

Lawrie A, Brisken AF, Francis SE, Cumberland DC, Crossman DC, Newman CM. Microbubble-enhanced ultrasound for vascular gene delivery. Gene Ther 2000;7:2023–2027.

Lawrie A, Brisken AF, Francis SE, Wyllie D, Kiss-Toth E, Qwarnstrom EE, Dower SK, Crossman DC, Newman CM. Ultrasound-enhanced transgene expression in vascular cells is not dependent upon cavitation-induced free radicals. Ultrasound Med Biol 2003;29:1453–1461.

Madanshetty SI, Roy RA, Apfel RE. Acoustic microcavitation: Its active and passive acoustic detection. J Acoust Soc Am 1991;90: 1515–1526.

Marmottant P, Hilgenfeldt S. Controlled vesicle deformation and lysis by single oscillating bubbles. Nature 2003;423:153–156.

Marmottant P, van der Meer S, Emmer M, Versluis M, de Jong N, Hilgenfeldt S, Lohse D. A model for large amplitude oscillations of coated bubbles accounting for buckling and rupture. J Acoust Soc Am 2005;118:3499–3505.

McNeil PL. Incorporation of macromolecules into living cells. Method Cell Biol 1989;29:153–173.

Mehier-Humbert S, Bettinger T, Yan F, Guy RH. Plasma membrane poration induced by ultrasound exposure: Implication for drug delivery. J Control Release 2005;104:213–222.

Miller DL, Bao S, Gies RA, Thrall BD. Ultrasonic enhancement of gene transfection in murine melanoma tumors. Ultrasound Med Biol 1999;25:1425–1430.

Miller DL, Dou C, Song J. DNA transfer and cell killing in epidermoid cells by diagnostic ultrasound activation of contrast agent gas bodies *in vitro.* Ultrasound Med Biol 2003;29:601–607.

Miller DL, Song J. Tumor growth reduction and DNA transfer by cavitation-enhanced high-intensity focused ultrasound *in vivo.* Ultrasound Med Biol 2003;29:887–893.

Mukherjee D, Wong J, Griffin B, Ellis SG, Porter T, Sen S, Thomas J. Ten-fold augmentation of endothelial uptake of vascular endothelial growth factor with ultrasound after systemic administration. J Am Coll Cardiol 2000;35:1678–1686.

Nyborg WL. Intermediate Biophysical Mechanisms. Menlo Park, CA: Cummings Publishing Co., 1975.

Prentice P, Cuschieri A, Dholakia K, Prausnitz MR, Campbell P. Membrane disruption by optically controlled microbubble cavitation. Nat Phys 2005;1:107–110.

Preston RC, Bacon DR, Livett AJ, Rajendran K. PVDF membrane hydrophone performance properties and their relevance to the measurement of the acoustic output of medical ultrasound equipment. J Phys E Sci Instr 1983;16:786–796.

Prosperetti A. A new mechanism for sonoluminescence. J Acoust Soc Am 1997;101:2003–2007.

Raum K, O'Brien WD Jr. Pulse-echo field distribution measurements technique for high-frequency ultrasound sources. IEEE Trans Ultrason Ferroelectr Freq Control 1997;44:810–815.

Rooney JA. Hemolysis near and ultrasonically pulsating gas bubble. Science 1970;169:869–871.

Rooney JA. Shear as a mechanism for sonically induced biological effects. J Acoust Soc Am 1972;52:1718–1724.

Schlicher RK, Radhakrishna H, Tolentino TP, Apkarian RP, Vladimir Z, Prausnitz MR. Mechanism of intracellular delivery by acoustic cavitation. Ultrasound Med Biol 2006;32:915–924.

Suslick KS. Sonochemistry and Sonoluminescence. In: Encyclopedia of Physical Science and Technology, vol 17, ed 3. San Diego, CA: Academic Press, 2001:363–376.

Tachibana K, Uchida T, Ogawa K, Yamashita N, Tamura K. Induction of cell membrane porosity by ultrasound. Lancet 1999;353:1409.

Taniyama Y, Tachibana K, Hiraoka L. Development of safe and efficient novel nonviral gene transfer using ultrasound: Enhancement of transfection efficiency of naked plasmid DNA in skeletal muscle. Gene Ther 2002;9:372–380.

Tata DB, Dunn F, Tindall DJ. Selective clinical ultrasound signals mediate differential gene transfer and expression in two human prostate cancer cell lines: LnCap and PC-3. Biochem Biophys Res Commun 1997;234:64–67.

Tran TA, Roger S, Le Geunnec JY, Tranquart F, Bouakaz A. Effect of ultrasound-activated microbubbles on the cell electrophysiological properties. Ultrasound Med Biol 2007;33:158–163.

van Wamel A, Bouakaz A, Bernard B, ten Cate F, de Jong N. Radionuclide tumour therapy with ultrasound contrast microbubbles. Ultrasonics 2004;42:903–906.

Weimann LJ, Wu J. Transdermal delivery of poly-l-lysine by sonomacroporation. Ultrasound Med Biol 2002;28:1173–1180.

Williams AR, Hughes DE, Nyborg WL. Hemolysis near a transversely oscillating wire. Science 1970;169:871–873.

Wu J, Pepe J, Rincón M. Sonoporation, anti-cancer drug and antibody delivery using ultrasound. Ultrasonics 2006;44:e21–e25.

Wu J, Ross JP, Chiu J. Reparable sonoporation generated by microstreaming. J Acoust Soc Am 2002;111:1460–1464.

Wyber JA, Andrews J, D'Emanuele A. The use of sonication for the efficient delivery of plasmic DNA into cells. Pharm Res 1997;14:750–756.

Zachary JF, Sepsrott JM, Frizzell LA, Simpson DG, O'Brien WD Jr. Superthreshold behavior and threshold estimation of ultrasound-induced lung hemorrhage in adult mice and rats. IEEE Trans Ultrason Ferroelectr Freq Control 2001;34:581–592.